GEOPHYSICAL RESEARCH LETTERS, VOL. 27, NO. 12, PAGES 1699-1702, JUNE 15, 2000

Tropospheric wind and humidity derived from spaceborne radar intensity and phase observations

Ramon Hanssen

Delft Institute for Earth-Oriented Space Research, Delft University of Technology, Delft, The Netherlands

Ilona Weinreich and Susanne Lehner

German Aerospace Research Establishment (DLR), Oberpfaffenhofen, Germany

Ad Stoffelen

Royal Netherlands Meteorological Institute, De Bilt, The Netherlands

Abstract. Causal connections between mesoscale wind patterns and moisture distribution in the lower boundary layer can be studied using satellite synthetic aperture radar (SAR) observations. Wind information is retrieved from radar backscatter intensity over water areas, whereas the moisture distribution is reflected in the radar signal delay. The latter can only be observed over land areas, using the interferometric combination of two radar images. This paper reports on the relation between wind and moisture associated with boundary layer rolls and with a cold-frontal rain band. The combination of both signals, originating from one sensor, is used to infer a quantitative description of the underlying dynamical processes.

Introduction

The purpose of this study is to present an extension to the technique of water vapor mapping, which was published in a recent paper [*Hanssen et al.*, 1999]. In that paper it is shown how observations from synthetic aperture radar (SAR) interferometry can be used to extract information on the moisture distribution in the boundary layer. Here we demonstrate how the same radar observations can also be used for wind field measurements, which enables an integrated analysis of wind and moisture parameters from a single sensor. Since mesoscale surface winds modulate fluxes of momentum, heat, and moisture—the driving forces of atmospheric circulation—there is close correpondence between the wind field and the transport and distribution of moisture. Examples include, e.g., cumulus convection and atmospheric dynamics near fronts. Improved understanding of both spatial and temporal behavior of air masses is important for parameterizations in weather forecasting and climate models.

Current observation methods are often limited in the spatial resolution they provide. Moreover, radiometric water vapor observations from contemporary meteorological satellites usually originate from atmospheric layers above 3 km, due to the strong absorption by water vapor [*Weldon and Holmes*, 1991]. This often restricts quantitative interpretation to upper tropospheric moisture distribution [*Schmetz et al.*, 1995]. Generally, basic meteorological parameters such as wind velocity and water vapor distribution are not measured on km-scales (see, e.g., *Stoffelen* [1998] for wind measurents and *Susskind et al.* [1984] for temperature and humidity information). A related problem is that wind and moisture observations are usually acquired by different sensors, that don't necessarily coincide in time. For the analysis of causal connections between both types of parameters on scales between 100 m and 10 km, temporal coincidence is imperative due to their spatial and temporal variability.

In this paper we elaborate on two case studies, previously presented in *Hanssen et al.* [1999], where we exploit both the radar backscatter intensity and phase information. This approach provides a more thorough examination of previous findings, which were based on phase information only. Using two pairs of interferometric SAR observations the moisture distribution over land areas is retrieved from the interferometric phase, whereas wind information is retrieved from the backscattered radar energy over water areas. The case studies constitute a comprehensive quantitative examination of vortices associated with a system of boundary layer rolls and with a rain band in relation to a cold front.

Methodology and data analysis

Spaceborne SAR provides fine-resolution radar images over broad areas. The pixel size in the ERS images analyzed here is ∼20 m over a swath of 100 km in width. The radar data comprise a grid of complex vectors, one for every pixel. The length of the vector is a measure for the backscatter intensity and yields information on the roughness of the imaged surface. Over water surfaces, the backscatter intensity is dominated by Bragg scattering. Contrasts in surface roughness, quantified in the normalized radar cross section (σ^0), can be interpreted as differences in mainly wind speed and direction [*Stoffelen*, 1998]. Sea state or heavy rain are further atmospheric phenomena which may influence the intensity. SAR images can detail small scale structures over seas such as boundary layer rolls [*Alpers and Brümmer*, 1994]. Here we used a C-band model, CMOD4, to compute the wind speed from the normalized radar cross section and the incidence angle of the radar waves [*Stoffelen*, 1998]. This model correlates backscatter intensity with the wind at 10 m height (Other models correlate to a so-called neutral equiv-

Paper number 1999GL011012.
0094-8276/00/1999GL011012$05.00

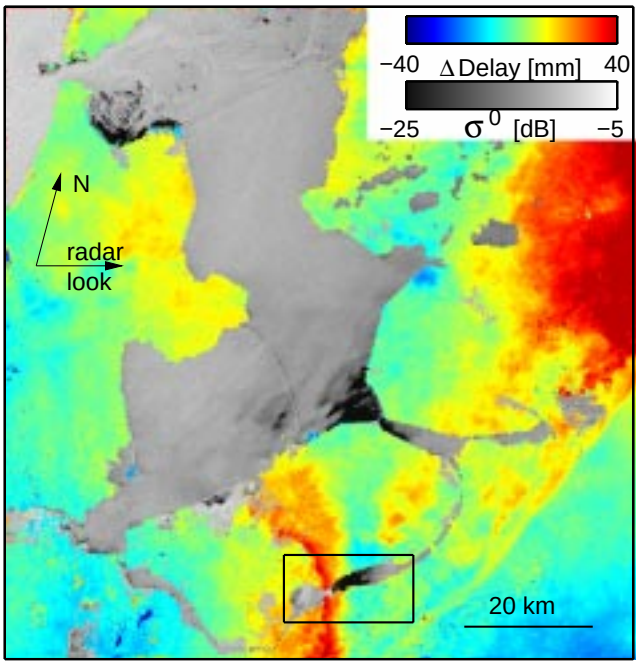

Figure 1. Differential SAR interferogram of a cold front, indicated by the diagonal line in the lower right corner. The area left of this line is the cold air mass (14°C), the area right is the warm air mass (17°C). Precipitation occurs only over the red areas in the interferogram. The curved feature in the lower part of the interferogram is a region with strong precipitation.

alent wind, but in that case accurate ancillary information is needed on atmospheric stratification [*Stoffelen*, 1998]).

The phase of the vector is a superposition of three components; a path length component, depending on the geometric distance between the spacecraft and the resolution cell, a propagation velocity component, and a scattering component due to the unknown reflection characteristics of the many different scatterers within a resolution cell. The superposition of the three components prohibits unambiguous interpretation of the phase measurement.

In the repeat-pass interferometric configuration, two SAR images are acquired from nearly the same position in space at two epochs, resulting in two nearly identical images. Differences in the phase information in both images are caused by the differences in the imaging geometry (different path lengths) and the different distribution of propagation delay during the first and the second acquisition. The scattering components over land and ice surfaces can be similar for both acquisitions, especially for short intervals. This principle enables the formation of a coherent phase-difference image or interferogram, see, e.g., *Bamler and Hartl* [1998] and *Massonnet and Feigl* [1998]. Here we eliminate phase signal due to geometric path length differences using an elevation model [*Massonnet et al.*, 1993]. As the interferometric pairs are acquired with a time interval of only 24 hours, coherent phase information is obtained in which no surface deformation occurred. This methodology ensures that the interferometric phase is only due to atmospheric propagation delay.

The delay of the radar signal is caused by an integration over the refractive index of the propagation medium, along the line of sight. Horizontal and vertical heterogeneities in refractive index are influenced by the spatial distribution of water vapor, pressure, temperature, liquid water, and electron content. Yet, over distances less than ∼50 km, the main signal in the interferogram is due to water vapor, albeit temperature and liquid water can add some additional mm's of delay [*Hanssen et al.*, 1999]. Using surface temperature observations, the integrated water vapor signal can be converted to precipitable water—its liquid equivalent, when assuming a fixed vertical temperature profile [*Bevis et al.*, 1992].

Results

Case study 1: Precipitation and convection

An ERS-2 SAR image (orbit 2388, frame 1053) was acquired during a cold front passage over the Netherlands, on 4 October 1995. The interferometric combination with an

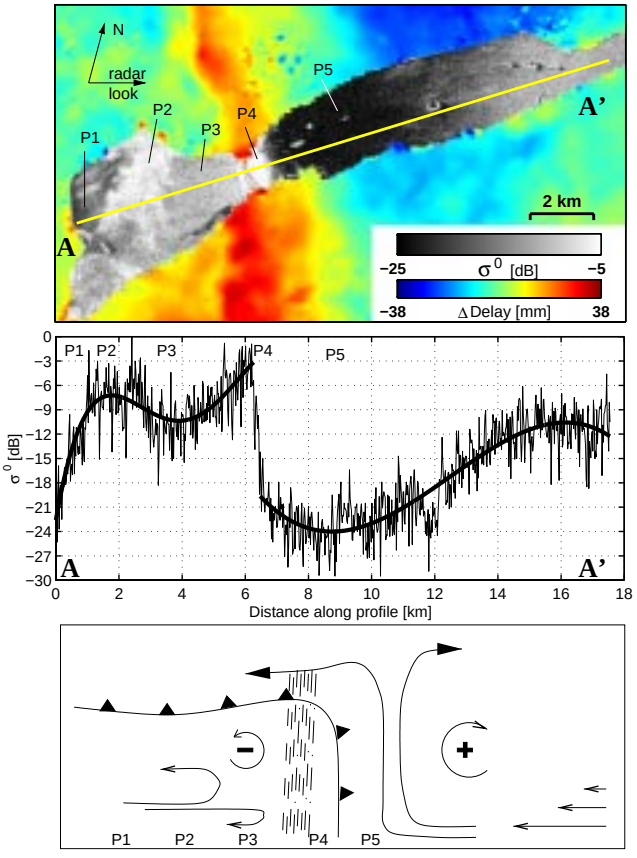

Figure 2. (a). Phase-intensity observations over Veluwe Lake, the Netherlands. The colored section shows interferometric phase observations, converted to slant signal delay variations in mm. The gray-scale part of the figure is derived from the backscatter intensity during the ERS-2 acquisition, and is scaled to logarithmic σ^0 values. The band with increased delay indicates strong rain, and is clearly correlated to the increased surface roughness over the water. (b) Cross section AA' of the radar cross section values in panel (a) The σ^0 values increase approximately 18 dB due to wind patterns associated with the storm. Behind the first rain band, indicated by label P4, roughness decreases and increases again, as observed in the first 6 km of the cross section. (c) Sketch of the circulation patterns associated with the cold front, after *Parsons* [1992]. The vertical shear in front of the storm consists of a windless area at the surface and probably a southwesterly wind aloft.

ERS-1 SAR image (orbit 22061), acquired 24 hours earlier, in the absence of significant weather in our target area, enabled the construction of a radar interferogram, see Figure 1. The figure shows coherent phase information over all land areas. Over the water area the intensity image of the SAR acquisition of 4 October is shown. The diagonal line in the lower right corner of the image is associated with the location of the cold front, and the curved anomaly in the center of the image can be associated with a gust front. Weather radar observations show strong precipitation in this region [*Hanssen et al.*, 1999].

Figure 2 shows a small section of this interferogram, centered over Veluwe Lake. The footprint of the storm is moving over the area from left to right. Over the land area, the increased humidity associated with the convective clouds and rain is measured as an increase in signal delay of approximately 30 mm. At this position, P4, weather radar observations indicated rain rates up to 10 mm/hr. In front of the storm (P5) the interferogram shows approximately uniform color, indicating not much variation in moisture. Behind the storm front (P3), variations in moisture are in the order of 8–12 mm, which can be associated with moisture variations due to, e.g., convective cells. The small circular anomalies near P5 are related to processing errors over single pixels.

The roughness of the water surface is expressed by the normalized radar cross section, σ^0, and is well correlated with the near-surface wind conditions [*Stoffelen*, 1998]. It is likely that the signatures on the water surface are mostly due to wind effects, as the signature of the rain would cause fine scale structures. Moreover, the rain rate is probably too low and the wind speed likely too high for there to be a rain effect by impact on the water surface. A cross-section of panel (a) is shown in panel (b). Collocated with the rain band, an increase in σ^0 of approximately 18 dB can be observed, at position P4. To the east of the storm front (P5) the water surface is relatively smooth. Moving towards the west, from P4 to P2, the roughness first decreases approximately 8 dB, (P3), to increase approximately 4 dB at P2. This nearly symmetrical wind shear appears to be closely associated with the storm front. Assuming a wind direction somewhere between upwind and crosswind, which are the horizontal or vertical directions in panel (a) the wind velocities following from CMOD4 are $\sim$0 m s^{-1} in front of the storm, P5, increasing up to $\sim$15 m s^{-1} in the storm, P4, within a spatial distance of 300 m.

At P4, there is a surplus of water vapor with respect to the surroundings, resulting in an excess delay of 3.6 cm, which corresponds to 5.3 $\pm$ 0.5 mm integrated precipitable water. The width of the main rain band is 2 km.

From wind observations and common circulation patterns in high-latitude convective systems, one can infer that the radar look direction is crosswind to the flow at location P5 in panel (a), and parallel to the rain band. Behind the rain band, P1–P3, the wind is more along the radar look direction and probably veering. More to the northeast of the rain band surface measurements indicate that the wind has also a component along the radar look direction. This means that besides wind speed changes, there are also wind direction changes that may be relevant for the signature in the radar image (P1–P5). The radar is most sensitive to wind direction changes for wind directions at 45, 135, 225, and 315 with respect to the radar look direction, whereas there is no sensitivity at 0, 90, 180, and 270 degrees.

From these observations, we find a circulation pattern connected to this system termed 'optimal shear' by [*Parsons*, 1992], depicted in panel (c), where in our case the complete system moves to the east, such that the vertical shear in front of the storm consists of an area with no wind at the surface and probably SW-winds aloft.

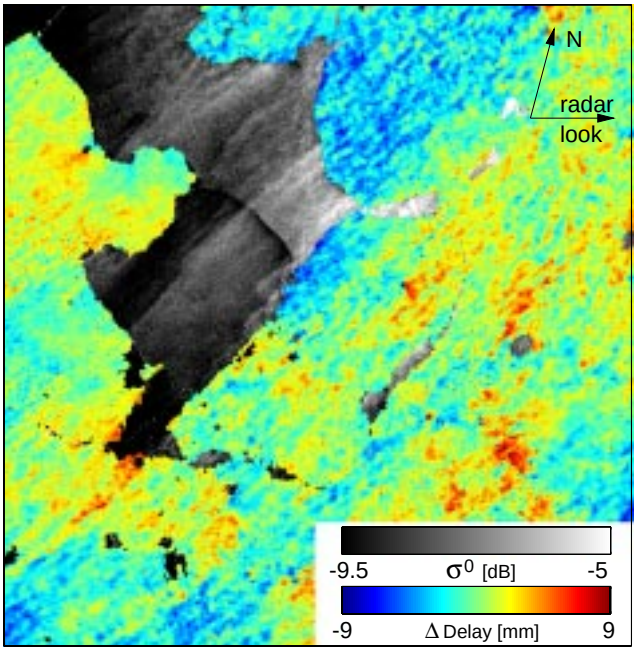

Figure 3. Radar intensity observations over IJssel Lake on 4 April 1996, 10:35 UTC, combined with signal delay differences derived from the interferometric phase between 4 and 5 April 1996. The signal in the interferometric phase is mainly due to water vapor differences between the moist updraft and the dryer downdraft regions *Weckwerth et al.* [1996]. The signal in the intensity observations over water is due to variations in the wind speed, and to a lesser extend wind direction, associated with the rolls.

Case study 2: Boundary layer rolls

During an ERS-1 acquisition on 4 April 1996, 10:34 UTC (orbit 24688, frame 2547), convective rolls occurred in the boundary layer [*Hanssen et al.*, 1999]. In the interferogram with an ERS-2 acquisition on 5 April 1996 (orbit 5015), see Figure 3, these rolls are clearly visible over the land areas. Since no clouds were observed at the surface stations in the area, the delay variation is a clear air effect.

Several studies have indicated that the ascending parts of the rolls transport warm, moist air at the surface upward, while the descending parts transport dry air originating witin the inversion downward, see, e.g. *LeMone* [1973]. *Weckwerth et al.* [1996] observed variations in the water vapor mixing ratio of 1.5–2.5 g/kg associated with rolls, whereas temperature variations were only 0.5 K. Mapped to water vapor pressure, these moisture variation are 2.4–4 hPa. The sensitivity of the delay to a 1 hPa change in water vapor pressure is in this situation at least 3.5 times as large as to a 1 K change in temperature. The delay variations of up to 10 mm are therefore dominantly caused by water vapor differences in the updraft and downdraft branches of the rolls. Not more than 5% of the observed delay can be explained by the temperature variations in the

rolls. The rolls are approximately parallel to the wind direction, and the wind speed observed at several surface stations is 6.2–7.7 m s^{-1}.

Over the water areas in IJssel lake, wind streaks are clearly visible, oriented in the same direction as the rolls over land areas. Although streaks caused by rolls are frequently observed in SAR images, see *Alpers and Brümmer* [1994], *Mourad and Walter* [1996], the location of the streaks with respect to the downdraft and updraft branches has been uncertain. Spectral analysis reveals a streak spacing of approximately 2 km. Over land, the spacing between the bands is also approximately 2–3 km. A radiosonde in the area, launched 90 minutes after the SAR acquisition, indicated a boundary layer depth of 800 m, which gives an aspect ratio of 2.5–2.9, typically for rolls [*Atkinson and Zhang*, 1996].

For wind speed estimation with a $\pm$1–2 m s^{-1} accuracy, an averaging area of 25 km^2 is needed [*Lehner et al.*, 1998]. Using square areas of 10 $\times$ 10 km, average wind speeds of 5.3–5.9 m s^{-1} were found. For the analysis of the wind speed differences between the streaks, square areas of this size cannot be used. Instead, we applied a normalized Radon transform to two areas of 11×11 km and used a profile perpendicular to the streaks to estimate the average differences in σ^0. This method reduces speckle effects significantly and enables direction dependent amplitude estimation. Variations over a range of 0.4–0.5 dB are observed, corresponding with wind speed variations of 1 m s^{-1} or wind direction variations of up to 45 degrees (i.e., the sensitivity to lateral wind velocity changes is about four times the sensitivity to transverse velocity variations).

We note the change in characteristics of the boundary layer rolls as they are advected over the cold water surface, where the fluxes of momentum and heat are expectedly quite different from those over land areas that are heated by the sun. The combination of measurements shown in this paper is ideally suited to show the transformation of air flow after advection over a land-water boundary.

The location of the streaks aligns approximately with the part of the rolls which have less delay, which correspond to the relatively dry and descending air. This is in correspondance with classical theory, which expects the maximum wind speed in a roll in the downdraft area [*Alpers and Brümmer*, 1994; *Atkinson and Zhang*, 1996]. Midlatitude cases, without cloud and with important dynamical and thermal instability, such as presented here, are uniquely documented by the SAR methodology presented here.

Discussion

The possibility to simultaneously combine both radar intensity observations over water and phase observations over land surfaces enables specific studies on the interrelation between moisture distribution and wind fields. The fine spatial resolution is particularly suitable for the study of mesoscale shallow convection in the planetary boundary layer in coastal areas or areas with large lakes to describe for example the transformation of air across the land-water interface. Although the phase delay measurements are always a summation of the delay during two acquisitions, specific patterns can often be recognized and analyzed.

Acknowledgments. The ERS SAR data were kindly provided by ESA. Part of the work was funded by the German Ministry of Research (BMBF) under contract number 03F0165C. T. Weckwerth provided valuable help in the meteorological interpretation. The meteorological data were made available by the Royal Netherlands Meteorological Institute (KNMI). We thank two anonymous reviewers for their critical comments.

References

Alpers, W., and B. Brümmer, Atmospheric boundary layer rolls observed by the synthetic aperture radar aboard the ERS-1 satellite, *Journal of Geophysical Research*, *99*, 12,613–12,621, 1994.

Atkinson, B. W., and J. W. Zhang, Mesoscale shallow convection in the atmosphere, *Reviews of Geophysics*, *34*, 403–431, 1996.

Bevis, M., S. Businger, T. A. Herring, C. Rocken, R. A. Anthes, and R. H. Ware, GPS meteorology: Remote sensing of atmospheric water vapor using the Global Positioning System, *Journal of Geophysical Research*, *97*, 15,787–15,801, 1992.

Hanssen, R. F., T. M. Weckwerth, H. A. Zebker, and R. Klees, High-resolution water vapor mapping from interferometric radar measurements, *Science*, *283*, 1295–1297, 1999.

Lehner, S., J. Horstmann, W. Koch, and W. Rosenthal, Mesoscale wind measurements using recalibrated ERS SAR images, *Journal of Geophysical Research*, *103*, 7847–7856, 1998.

Massonnet, D., M. Rossi, C. Carmona, F. Adagna, G. Peltzer, K. Feigl, and T. Rabaute, The displacement field of the Landers earthquake mapped by radar interferometry, *Nature*, *364*, 138–142, 1993.

Parsons, D. B., An explanation for intense frontal updrafts and narrow cold-frontal rainbands, *Journal of the Atmospheric Sciences*, *49*, 1810–1825, 1992.

Schmetz, J., W. Menzel, C. Velden, X. Wu, L. van de Berg, S. Nieman, C. Hayden, K. Holmlund, and C. Geijo, Monthly mean large-scale analyses of upper-tropospheric humidity and wind field divergence derived from three geostationary satellites, *Bulletin of the American Meteorological Society*, *76*, 1578–1584, 1995.

Stoffelen, A. C. M., Scatterometry, Ph.D. thesis, Utrecht University, 1998, ISBN: 90-393-1708-9.

Weckwerth, T. M., J. W. Wilson, and R. M. Wakimoto, Thermodynamic variability within the convective boundary layer due to horizontal convective rolls, *Monthy Weather Review*, *124*, 769–784, 1996.

Weldon, R. B., and S. J. Holmes, Water vapor imagery interpretation and applications to weather analysis and forecasting., *Tech. Rep. NESDIS 57*, NOAA, 1991.

R.F. Hanssen, DEOS, Delft University of Technology, Thijsseweg 11, 2629 JA, Delft, The Netherlands. (e-mail: hanssen@geo.tudelft.nl)

I. Weinreich, S. Lehner, Deutsches Zentrum für Luft- und Raumfahrt (DLR) e.V., Oberpfaffenhofen, D-82234 Wessling, Germany. (e-mail: Ilona.Weinreich@dlr.de; Susanne.Lehner@dlr.de)

A.C.M. Stoffelen, KNMI, Postbus 201, 3730 AE de Bilt, The Netherlands. (e-mail: Ad.Stoffelen@knmi.nl)

(Received August 17, 1999; revised February 27, 2000; accepted March 7, 2000.)